Hindawi
Advances in Materials Science and Engineering
Volume 2018, Article ID 5436020, 8 pages
https://doi.org/10.1155/2018/5436020

Research Article

3D Simulation of Self-Compacting Concrete Flow Based on MRT-LBM

Liu-Chao Qiu and Yu Han

College of Water Resources and Civil Engineering, China Agricultural University, Beijing 100083, China

Correspondence should be addressed to Liu-Chao Qiu; qiuliuchao@cau.edu.cn and Yu Han; yh916@uowmail.edu.au

Received 21 June 2017; Accepted 2 November 2017; Published 28 January 2018

Academic Editor: Ying Li

A three-dimensional multiple-relaxation-time lattice Boltzmann method (MRT-LBM) with a D3Q27 discrete velocity model is applied for simulation of self-compacting concrete (SCC) flows. In the present study, the SCC is assumed as a non-Newtonian fluid, and a modified Herschel–Bulkley model is used as constitutive mode. The mass tracking algorithm was used for modeling the liquid-gas interface. Two numerical examples of the slump test and enhanced L-box test were performed, and the calculated results are compared with available experiments in literatures. The numerical results demonstrate the capability of the proposed MRT-LBM in modeling of self-compacting concrete flows.

1. Introduction

As a highly flowable concrete, the self-compacting concrete does not require any vibration during casting processes and has been considered as "the most revolutionary development in concrete construction for several decades" [1]. Although SCC has been successful in plenty of applications, many problems are encountered during construction because of aggregate segregation, air voids, and the improper filling of formworks, and most of these problems are closely related to the flowability of SCC. Therefore, it is important to well understand and accurately predict the flow characteristics for the success of SCC casting. However, the accurate prediction of the SCC flowing behavior is a big challenge, especially in the case of heavy reinforcement, complex formwork shapes, and large size of aggregates. In this regard, the numerical modeling of SCC is an indispensable and inexpensive approach, not only as a tool for form filling prediction but also in terms of determination of fresh concrete properties, mix design, and casting optimization. Nowadays, the numerical modeling of fresh concrete flow has gained importance, and it is becoming an important tool for the prediction and optimization of casting processes [2, 3].

The modeling of fresh SCC is not a trivial task because it involves a free-surface flow of a dense suspension with a wide range of particle sizes and shows non-Newtonian flow behavior. A complete description of SCC from the cement particles to coarse aggregates is impossible with any computer model since accounting for broad particle size and shape distributions exceeds the computational limits of even the best supercomputers [4]. The fresh SCC can be treated as a one-phase fluid and simulated using CFD because it is flowable and the amount of coarse particles is lower than that in conventional concrete. In terms of rheology, the fresh SCC can be approximated as one of the known non-Newtonian materials such as the Bingham or Herschel–Bulkley fluid. In case if the high shear rates are likely to occur in the casting processes, the shear-thickening behavior can happen, and the Herschel–Bulkley model could be a more suitable one. At the end of the casting process, the shear rates are rather low and the yield stress practically dominates the flow. Therefore, the material can be modeled as a Bingham fluid to predict the final shape.

At present, many numerical techniques have been developed to model the SCC flow by assuming it as a homogeneous viscous fluid and using either the mesh-based methods such as the finite volume method (FVM) [5] and the finite element method (FEM) [6] or the meshless methods like the smoothed particle hydrodynamics (SPH) and the lattice Boltzmann method (LBM). Due to the fact that the flow of SCC is a typical free-surface flow, the treatment of the interface and its position represents another

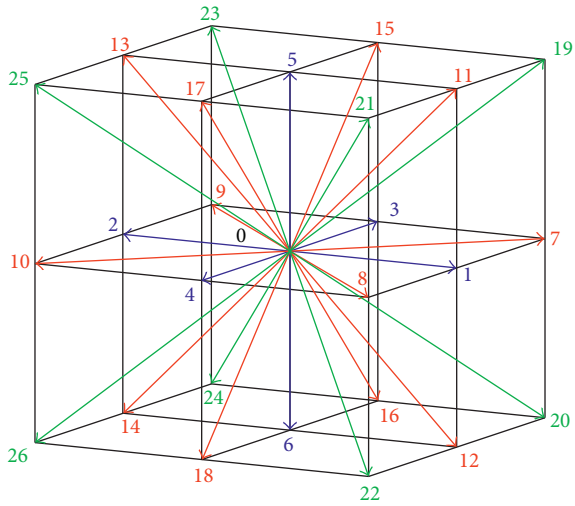

Figure 1: Three-dimensional twenty-seven particle velocity (D3Q27) lattice.

important numerical modeling issue. In this regard, the meshless methods have an advantage over the mesh-based methods. As a meshless Lagrangian method, the SPH method is good at modeling Newtonian and non-Newtonian flows with a free surface [7] and has been chosen for simulating the SCC flow by Kulasegaram et al. [8], Lashkarbolouk et al. [9], Qiu [10], Abo Dhaheer et al. [11], and Wu et al. [12]. However, the SPH method has difficulties in solving problems with complex solid boundary conditions. For these reasons, many researchers have made much effort to develop an alternative method called LBM for modeling the SCC flow due to the fact that it is easy for coding, intrinsically parallelizable, and applicable to complex geometries straightforwardly. For example, Švec et al. [13] and Leonardi et al. [14] simulated the fresh SCC as the non-Newtonian fluid based on the single-relaxation-time (SRT) LBM. Although the single-relaxation-time (SRT) model has been successful in many applications, it is prone to numerical instability in complex flows [15]. To overcome these difficulties, the multiple-relaxation-time (MRT) model proposed by d'Humiéres et al. [16] is useful to stabilize the solution and to obtain satisfactory results because the MRT model allows the usage of an independently optimized relaxation time for each physical process [17]. Therefore, Chen et al. [18] solved Bingham fluids by using the MRT model, but the free surface is not considered in their model. In the present work, we will develop a 3D multiple-relaxation-time LBM with a mass tracking algorithm representing the free surface to simulate the flow of fresh SCC.

2. Mathematical Formulations

2.1. Multiple-Relaxation-Time LBM. In this paper, the SCC flow is solved based on the lattice Boltzmann method which is considered as a very attractive alternative to the traditional CFD, especially in problems with complex boundary conditions. In the LBM, a finite number of velocity vectors $\mathbf{e}_\alpha$ are used to discretize the velocity space, and the fluid motion is described by a particle distribution function $f(\mathbf{x}, \mathbf{e}_\alpha, t)$ which is the probability density of finding particles with velocity $\mathbf{e}_\alpha$ at a location $\mathbf{x}$ and at a given time t. The LB equations can recover the continuum Navier–Stokes equations by means of the Chapman–Enskog expansion if a proper set of discrete velocities was employed [17, 19]. The D3Q27 (3 dimensions and 27 velocities) discrete velocity model illustrated in Figure 1 was used in this study. The particle velocity vectors $\mathbf{e}_\alpha$ for this lattice model are given by

$$\mathbf{e}_\alpha = \begin{cases} (0,0,0)c, & \alpha = 0, \\ (\pm 1,0,0)c,\ (0,\pm 1,0)c,\ (0,0,\pm 1)c, & \alpha = 1,\ldots,6, \\ (\pm 1,\pm 1,0)c,\ (\pm 1,0,\pm 1)c,\ (0,\pm 1,\pm 1)c, & \alpha = 7,\ldots,18, \\ (\pm 1,\pm 1,\pm 1)c, & \alpha = 19,\ldots,26, \end{cases} \tag{1}$$

where $c = \delta x/\delta t$, with δx and δt being the lattice spacing and the time step, respectively.

A discretization of the Boltzmann equation in time and space leads to the lattice Boltzmann equation [20, 21]:

$$f_\alpha(\mathbf{x} + \mathbf{e}_\alpha \delta t, t + \delta t) - f_\alpha(\mathbf{x}, t) = \Lambda_{\alpha j}\left[f_j(\mathbf{x}, t) - f_j^{\mathrm{eq}}(\mathbf{x}, t)\right] + F_\alpha \delta t, \tag{2}$$

where f_α is the distribution function of particles moving with velocity $\mathbf{e}_\alpha$, $\Lambda_{\alpha j}$ is the collision matrix, f^{eq} is the equilibrium distribution function, and F_α is the external force.

The equilibrium distribution function f^{eq} is obtained using the Taylor series expansion of the Maxwell–Boltzmann distribution function with velocity $\mathbf{u}$ up to second order. It can be written as

$$f_\alpha^{\mathrm{eq}} = \rho w_\alpha\left[1 + \frac{\mathbf{e}_\alpha \cdot \mathbf{u}}{c_s^2} + \frac{(\mathbf{e}_\alpha \cdot \mathbf{u})^2 - (c_s|\mathbf{u}|)^2}{2c_s^4}\right], \tag{3}$$

where ρ is the fluid density, $\mathbf{u}$ is the fluid velocity, and the sound speed is $c_s = c/\sqrt{3}$. The weight coefficients for D3Q27 are given by

$$w_\alpha = \begin{cases} \dfrac{8}{27}, & \alpha = 0, \\ \dfrac{2}{27}, & \alpha = 1,\ldots,6, \\ \dfrac{1}{54}, & \alpha = 7,\ldots,18, \\ \dfrac{1}{216}, & \alpha = 19,\ldots,26. \end{cases} \tag{4}$$

The components of $\mathbf{F}$ are given as

$$F_\alpha = w_\alpha \rho \frac{\mathbf{e}_\alpha \cdot \mathbf{a}}{c_s^2}, \tag{5}$$

where $\mathbf{a}$ is the acceleration.

The relaxation process has major influence on the physical fidelity as well as numerical stability. For the single-

relaxation-time (SRT) model, the collision matrix is $\Lambda_{\alpha j} = -1/\tau\delta_{\alpha j}$, where $\delta_{\alpha j}$ is the Kronecker symbol and τ is the relaxation time which is related to the kinetic viscosity by $\nu = c_s^2(\tau - 1/2)\delta t$. For the multiple-relaxation-time LBM, the collision matrix $\mathbf{\Lambda}$ can be written as [15]

$$\mathbf{\Lambda} = -\mathbf{M}^{-1}\mathbf{S}\mathbf{M}, \tag{6}$$

where the linear transform matrix $\mathbf{M}$ is a 27×27 matrix. The diagonal matrix $\mathbf{S}$ may be written as $\mathbf{S} = \text{diag}\,(0, 0, 0, 0, s4, s5, s5, s7, s7, s7, s10, s10, s10, s13, s13, s13, s16, s17, s18, s18, s20, s20, s20, s23, s23, s23, s26)$ with $s4 = 1.54$, $s5 = s7 = 1/\tau$, $s10 = 1.5$, $s13 = 1.83$, $s16 = 1.4$, $s17 = 1.61$, $s18 = s20 = 1.98$, and $s23 = s26 = 1.74$.

The macroscopic density ρ and velocity $\mathbf{u}$ are computed by

$$\rho = \sum_{\alpha=0}^{26} f_\alpha, \qquad \mathbf{u} = \sum_{\alpha=0}^{26} \mathbf{e}_\alpha f_\alpha + \frac{1}{2}\mathbf{a}\delta t. \tag{7}$$

The pressure p is related to the density by

$$p = \rho c_s^2. \tag{8}$$

2.2. Free Surface Modeling. For the modeling of the liquid-gas interface, the most straightforward way is to track all the phases, for example, liquid and gas. Such a method has the highest accuracy at the expense of high computational costs. The mass tracking algorithm [22] without considering the gas phase is employed in the present study due to the fact that it is simple, fast, and accurate. In this algorithm, the fluid domain is divided into liquid, interface, and gas nodes (Figure 2). The liquid and interface nodes are active and solved by the LBM, and the remaining gas nodes are inactive without evolution equation. Liquid and gas nodes are never directly connected but through an interface node. The adopted mass tracking algorithm is applied directly at the level of the LBM, so the algorithm mimics the free surface by modifying the particle distributions. An additional macroscopic variable for the mass $m(\mathbf{x}, t)$ stored in a node is required and defined as

$$\begin{aligned} &m(\mathbf{x}, t) = \rho(\mathbf{x}, t), && \text{for liquid nodes,} \\ &0 < m(\mathbf{x}, t) < \rho(\mathbf{x}, t), && \text{for interface nodes,} \\ &m(\mathbf{x}, t) = 0, && \text{for gas nodes.} \end{aligned} \tag{9}$$

The mass is calculated by

$$m(\mathbf{x}, t + \delta t) = m(\mathbf{x}, t) + \sum_\alpha k_\alpha \Big[f_{\bar{\alpha}}(\mathbf{x} + \mathbf{e}_\alpha \delta t, t) - f_\alpha(\mathbf{x}, t) \Big], \tag{10}$$

where $f_{\bar{\alpha}}$ and f_α are the particle distributions with opposite directions and

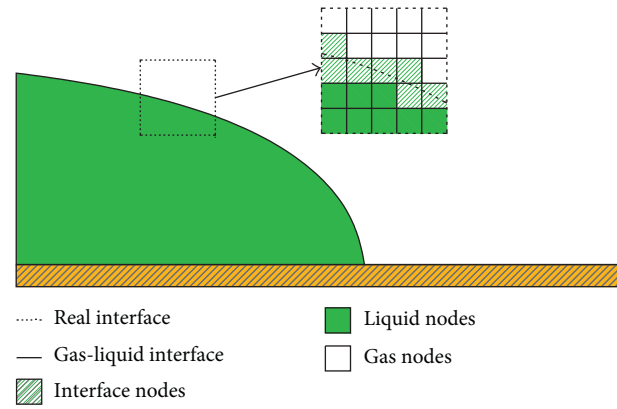

Figure 2: Mass tracking algorithm scheme.

$$k_\alpha = \begin{cases} \dfrac{[m(\mathbf{x}, t) + m(\mathbf{x} + \mathbf{e}_\alpha \delta t, t)]}{2}, & \text{for interface nodes,} \\ 1, & \text{for liquid nodes,} \\ 0, & \text{for gas nodes.} \end{cases} \tag{11}$$

The interface node becomes a fluid node when the mass reaches its density with $m(\mathbf{x}, t) = \rho(\mathbf{x}, t)$ and vice versa; the interface node becomes a gas node when the mass drops down to zero with $m(\mathbf{x}, t) = 0$.

2.3. Modified Herschel–Bulkley Model. In this study, the fresh SCC is assumed as viscoplastic fluids to consider its non-Newtonian behavior. Among the constitutive relations of viscoplastic fluids, the Herschel–Bulkley model is probably the most commonly used because of its simplicity and flexibility. The standard Herschel–Bulkley model is described by

$$\begin{aligned} &\dot{\gamma} = 0, && \sigma < \sigma_y, \\ &\sigma = \sigma_y + k\dot{\gamma}^n, && \sigma \geq \sigma_y, \end{aligned} \tag{12}$$

where $\dot{\gamma}$ is the shear rate (s^{-1}), σ is the stress (Pa), σ_y is the yield stress (Pa), and k is the consistency index (Pa·s^n); n is a measure of the deviation of the fluid from Newtonian (the power-law index). For a fluid with $n > 1$, the effective viscosity increases with shear rate, and the fluid is called shear-thickening or dilatant fluid. For a fluid with $0 < n < 1$, the effective viscosity decreases with shear rate, and the fluid is called shear-thinning or pseudoplastic fluid.

The standard Hershel–Bulkley model becomes discontinuous at less shear rates and causes instability during numerical solution due to the fact that the non-Newtonian viscosity becomes unbounded at small shear rates. In order to overcome such discontinuity, the standard Herschel–Bulkley model can be modified as [23]

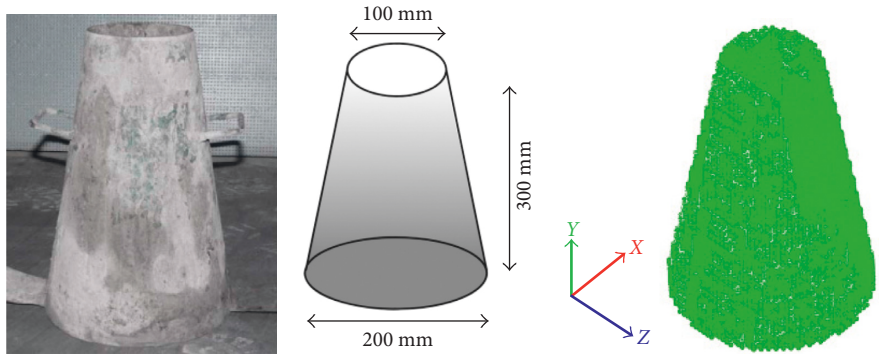

Figure 3: Slump test. (a) Experiment setup [24], (b) model size, and (c) LBM discretization.

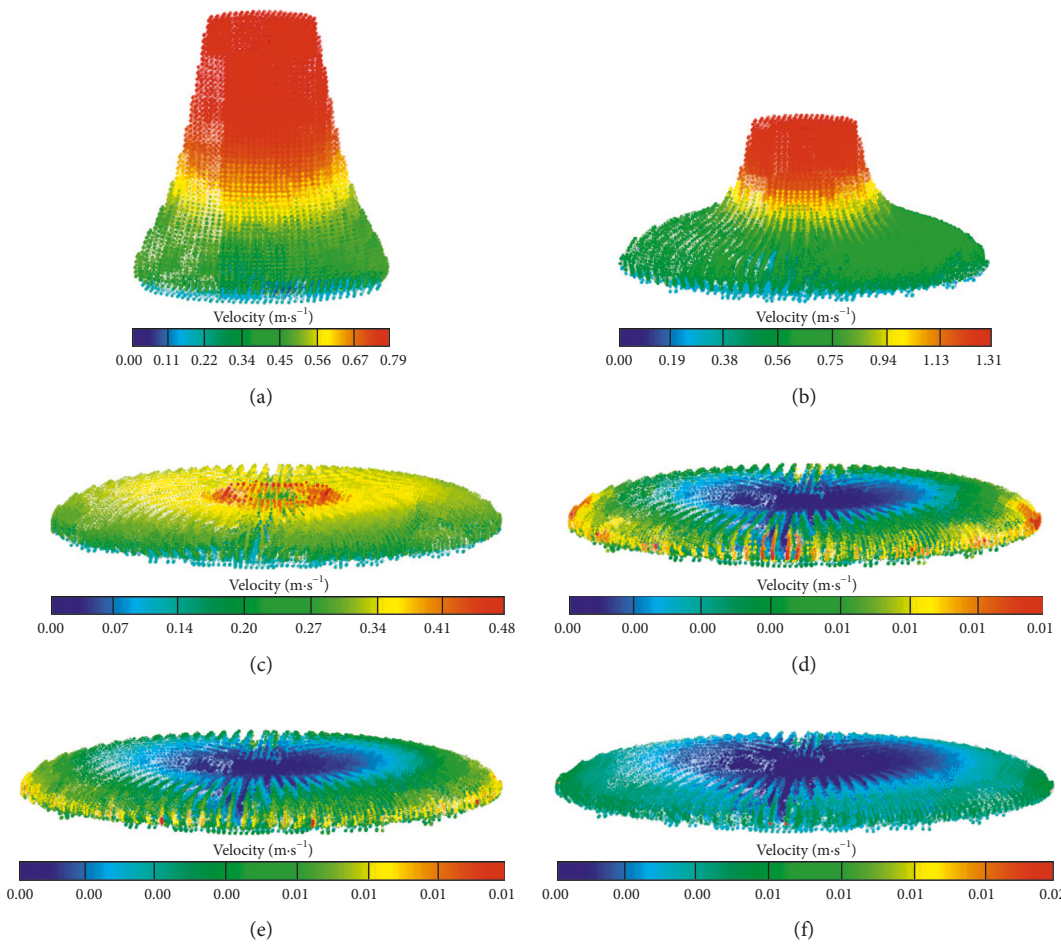

Figure 4: The velocity distribution during the slump test. (a) $t = 0.1$ s, (b) $t = 0.2$ s, (c) $t = 0.3$ s, (d) $t = 0.5$ s, (e) $t = 1.0$ s, and (f) $t = 2.0$ s.

$$\mu = \mu_y, \qquad \sigma < \sigma_y,$$
$$\mu = \frac{\sigma_y}{\dot{\gamma}} + \frac{k}{\dot{\gamma}}\left[\dot{\gamma}^n - \left(\frac{\sigma_y}{\mu_y}\right)^n\right], \qquad \sigma \geq \sigma_y, \tag{13}$$

where μ is the apparent viscosity of fluid, and the yielding viscosity μ_y can be estimated from experimental rheological curves and can be assumed to be the slope of the line of shear stress versus shear rate curve before yielding. The modified Herschel–Bulkley model combines the effects of Bingham and power-law behavior in a fluid. For low strain rates, the material acts like a very viscous fluid with yield viscosity μ_y. As the strain rate increases and the yield stress threshold σ_y is passed, the fluid behavior is described by a power law.

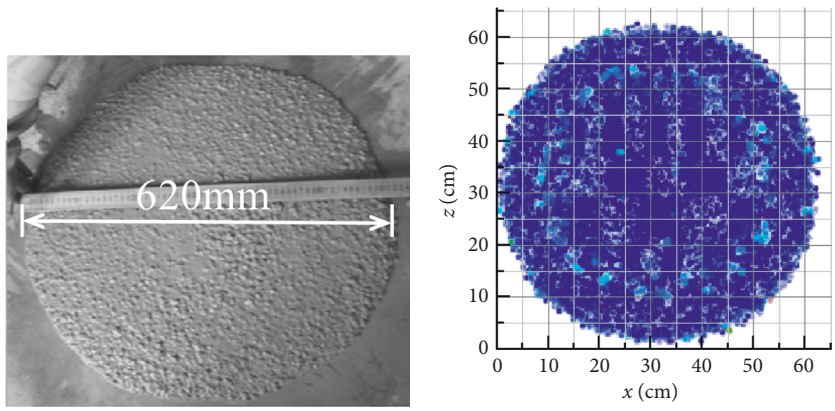

(a) (b)

Figure 5: Final spread of the slump test. (a) Experiment [24] and (b) simulation.

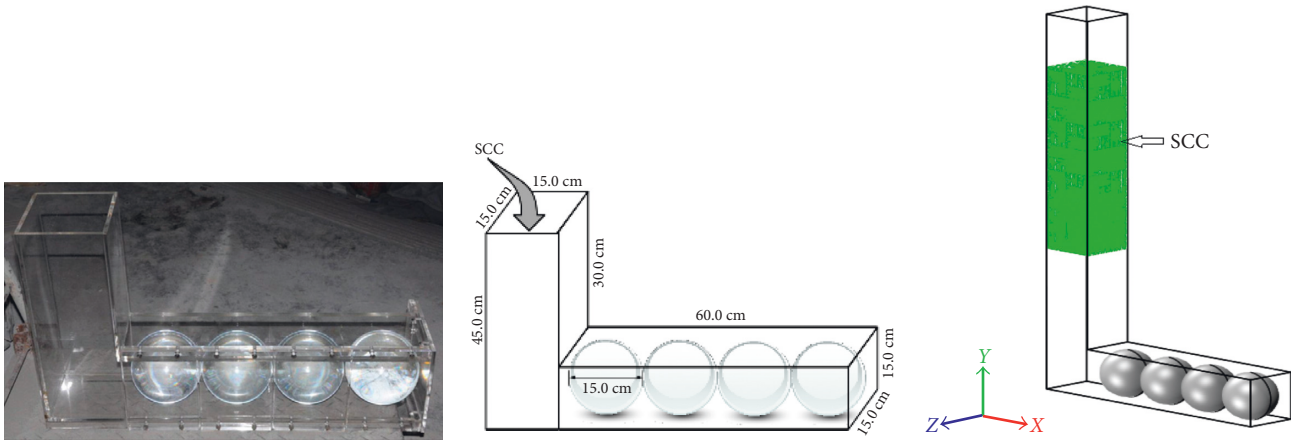

(a) (b) (c)

Figure 6: The enhanced L-box test. (a) Experiment setup [24], (b) model size, and (c) LBM discretization.

3. Numerical Examples and Validation

In this section, the developed MRT-LBM is applied to simulate the slump flow of fresh SCC to validate the capability of the proposed model in modeling SCC flow. And the model is also used to simulate the passing ability and the filling ability of SCC by using an enhanced L-box test.

3.1. Slump Test. The slump flow is the most commonly used test in SCC technology. It measures flow spread and optionally the flow time t_{50}. The numerical simulation of the slump test in our study is based on a laboratory experiment by Huang [24], Figure 3(a). The dimensions of the cone are 300 mm height, 200 mm lower diameter, and 100 mm upper diameter, Figure 3(b). The SCC used in this study has the following properties: yield stress = 100 Pa, plastic viscosity = 50 Pa·s, and density = 2300 kg/m^3. In the standard form of the slump test, only the final spread value of the slump is measured to evaluate the flowing behavior of the SCC.

The numerical simulation of the slump flow is performed based on the developed MRT-LBM. In our simulation, the lattice spacing is set to 0.01 m for the LBM discretization, Figure 3(c). The value of the yielding viscosity was chosen to be 1000 times higher than the value of the yield stress, with the power-law index being $n = 1$. Figure 4 presents some snapshots at different instants of the material shape with the velocity magnitude. In Figure 5, experimental and numerical results for the material shape at the end of the flow are compared. It can be seen from this figure that the calculated slump flow spread diameter is about 624 mm which shows a perfect match between the experimental and simulated flow distance that can be observed in terms of the maximum spread distance. This proves the correctness of the proposed model and its ability to simulate the free surface flow of fresh SCC.

3.2. Enhanced L-Box Test. The L-box test is generally used for assessing the passing ability and filling ability of fresh SCC in

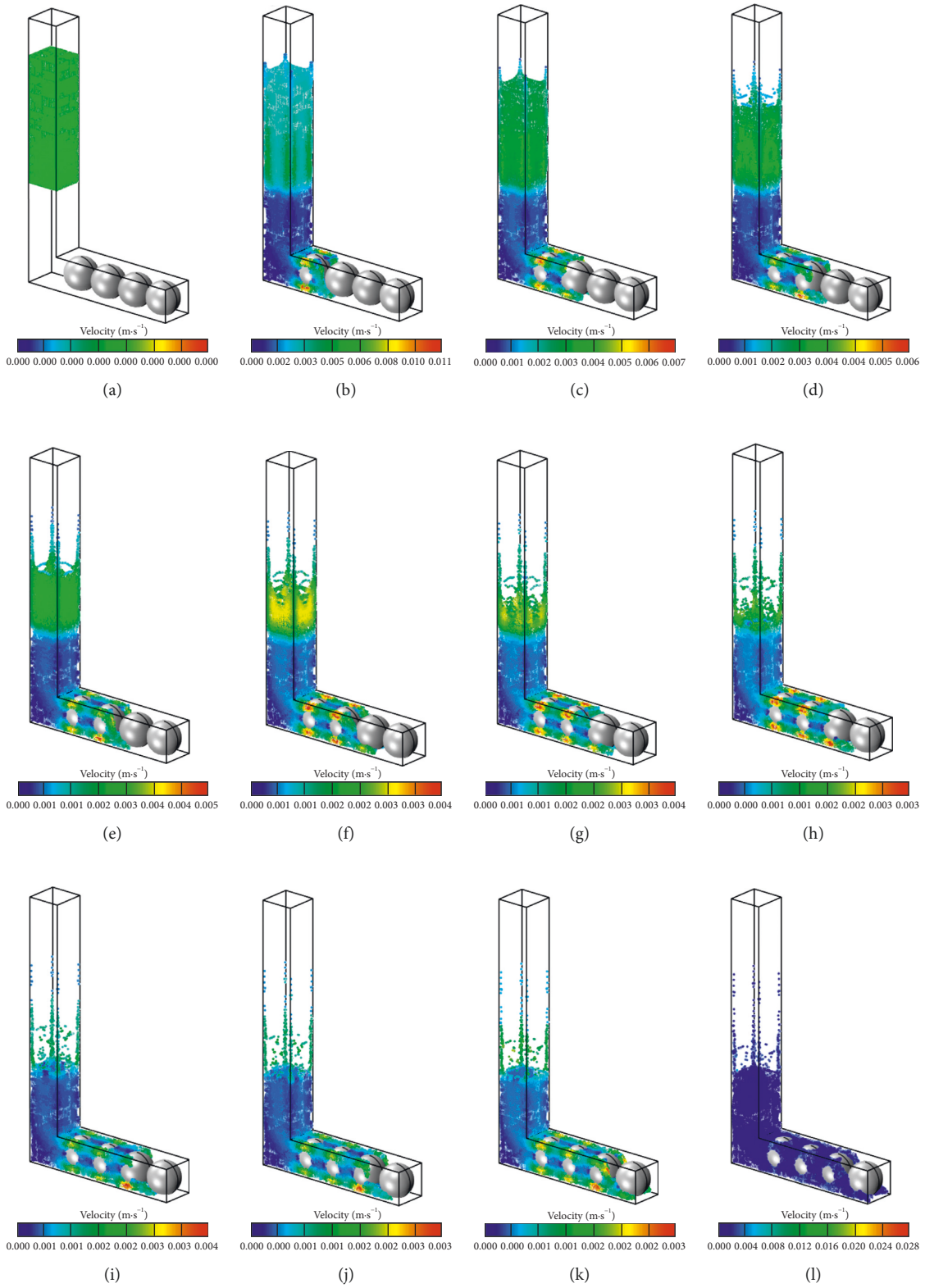

FIGURE 7: The velocity distribution of the enhanced L-box test. (a) $t = 0$ s, (b) $t = 25$ s, (c) $t = 50$ s, (d) $t = 75$ s, (e) $t = 100$ s, (f) $t = 125$ s, (g) $t = 150$ s, (h) $t = 175$ s, (i) $t = 200$ s, (j) $t = 225$ s, (k) $t = 250$ s, and (l) final shape.

confined spaces. In this section, a laboratory experiment of an enhanced L-box test by Huang [24] was simulated using the developed MRT-LBM. The enhanced L-box consists of the concrete reservoir, slide gate, and horizontal test channel with four ball obstacles (Figure 6(a)). The vertical section is filled with concrete, and subsequently, the gate is lifted to allow

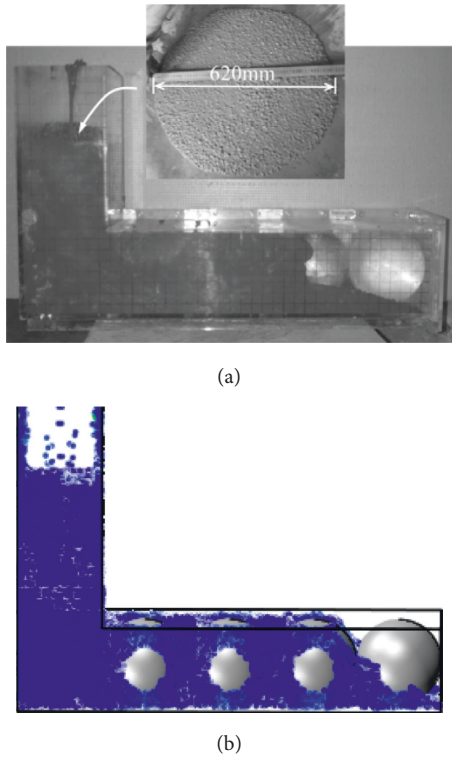

(a)

(b)

Figure 8: Final shape of SCC in the enhanced L-box test. (a) Experiment [24] and (b) simulation.

concrete to flow into the horizontal section. When the flow stops, one measures the reached height of fresh SCC after passing through the specified gaps of balls and flowing within a defined flow distance. With this reached height, the passing or blocking behavior of SCC can be estimated. The dimensions of the enhanced L-box test are shown in Figure 6(b).

In our simulation, the SCC is placed at the middle upper part of the vertical container, which is then suddenly released, and the concrete begins to spread under the gravity loading, Figure 6(c). The numerical simulation is performed based on the developed MRT-LBM and the lattice spacing is set to 0.01 m for the LBM discretization. The value of the yielding viscosity was chosen to be 1000 times higher than the value of the yield stress, with the power-law index being $n = 1$. SCC used for this study was the same concrete as in the slump test with the following properties: yield stress = 50 Pa, plastic viscosity = 50 Pa·s, and density = 2300 kg/m^3. The total volume of the material is $V = 13$ L. Some snapshots of the SCC shape with the velocity magnitude at different instants are presented in Figure 7. Figure 8 compares the experimental and numerical results for the final spread of the SCC flow. The simulated flow spread agrees well with the experimental results. This in turn further validates the proposed model in modeling the passing ability and filling ability of fresh SCC in confined spaces. A slight discrepancy in the shape of the SCC can be noted which may be due to the fact that the balls are perfectly touched by the lateral wall in simulation but there are existing gaps between them in the experiment.

4. Conclusions

In this paper, a multiple-relaxation-time LBM with a D3Q27 discrete velocity model for modeling the flow behavior of fresh SCC was proposed. The rheology of the fresh SCC was approximated as a non-Newtonian material using the modified Herschel–Bulkley fluid model. The free surface was modeled based on the mass tracking algorithm which is a simple and fast algorithm that conserves the mass precisely. The numerical simulation of slump flow of fresh SCC was first performed to validate the capability of the proposed model in modeling SCC flow. And then, the model was further used to simulate the passing ability and the filling ability of fresh SCC in confined spaces based on an enhanced L-box test. The simulated results agree well with the corresponding experimental data in the published literature. This proves that the proposed MRT-LBM is suitable for numerical simulations of the fresh SCC flows. It should be noted that the main problem for the application of the present model to real engineering problems is its high computational cost. Therefore, further investigations might be needed to consider hardware acceleration and parallel computing to make the proposed model more useful and versatile.

Conflicts of Interest

The authors declare that they have no conflicts of interest.

Acknowledgments

The authors are grateful for funding from the National Natural Science Foundation of China (Grant nos. 11772351 and 51509248) and the Scientific Research and Experiment of Regulation Engineering for the Songhua River Mainstream in Heilongjiang Province, China (Grant no. SGZL/KY-12).

References

[1] EFNARC, *Specification and Guidelines for Self-Compacting Concrete*, Scientific Research Publishing, Surrey, UK, 2002.

[2] N. Roussel, M. R. Geiker, F. Dufour, L. N. Thrane, and P. Szabo, "Computational modeling of concrete flow: general overview," *Cement and Concrete Research*, vol. 37, no. 9, pp. 1298–1307, 2007.

[3] N. Roussel and A. Gram, *Simulation of Fresh Concrete Flow, State-of-the Art Report of the RILEM Technical Committee 222-SCF, RILEM State-of-the-Art Reports*, vol. 15, Springer, Netherlands, 2014.

[4] K. Vasilic, M. Geiker, J. Hattel et al., "Advanced Methods and Future Perspectives," in *Simulation of Fresh Concrete Flow*, N. Roussel and A. Gram, Eds., vol. 15pp. 125–146, Springer, Netherlands, 2014.

[5] N. Roussel, "Correlation between yield stress and slump: comparison between numerical simulations and concrete rheometers results," *Materials and Structures*, vol. 39, no. 4, pp. 501–509, 2006.

[6] B. Patzák and Z. Bittnar, "Modeling of fresh concrete flow," *Computers and Structures*, vol. 87, no. 15, pp. 962–969, 2009.

[7] S. Shao and E. Y. M. Lo, "Incompressible SPH method for simulating Newtonian and non-Newtonian flows with a free surface," *Advances in Water Resources*, vol. 26, no. 7, pp. 787–800, 2003.

[8] S. Kulasegaram, B. L. Karihaloo, and A. Ghanbari, "Modelling the flow of self-compacting concrete," *International Journal for Numerical and Analytical Methods in Geomechanics*, vol. 35, no. 6, pp. 713–723, 2011.

[9] H. Lashkarbolouk, M. R. Chamani, A. M. Halabian, and A. R. Pishehvar, "Viscosity evaluation of SCC based on flow simulation in L-box test," *Magazine of Concrete Research*, vol. 65, no. 6, pp. 365–376, 2013.

[10] L.-C. Qiu, "Three dimensional GPU-based SPH modelling of self-compacting concrete flows," in *Proceedings of the third international symposium on Design, Performance and Use of Self-Consolidating Concrete*, pp. 151–155, RILEM Publications S.A.R.L, Xiamen, China, June 2014.

[11] M. S. Abo Dhaheer, S. Kulasegaram, and B. L. Karihaloo, "Simulation of self-compacting concrete flow in the J-ring test using smoothed particle hydrodynamics (SPH)," *Cement and Concrete Research*, vol. 89, pp. 27–34, 2016.

[12] J. Wu, X. Liu, H. Xu, and H. Du, "Simulation on the self-compacting concrete by an enhanced Lagrangian particle method," *Advances in Materials Science and Engineering*, vol. 2016, Article ID 8070748, 11 pages, 2016.

[13] O. Švec, J. Skoček, H. Stang, M. R. Geiker, and N. Roussel, "Free surface flow of a suspension of rigid particles in a non-Newtonian fluid: a lattice Boltzmann approach," *Journal of Non-Newtonian Fluid Mechanics*, vol. 179–180, pp. 32–42, 2012.

[14] A. Leonardi, F. K. Wittel, M. Mendoza, and H. J. Herrmann, "Coupled DEM-LBM method for the free-surface simulation of heterogeneous suspensions," *Computational Particle Mechanics*, vol. 1, no. 1, pp. 3–13, 2014.

[15] K. N. Premnath and S. Banerjee, "On the three-dimensional central moment Lattice Boltzmann method," *Journal of Statistical Physics*, vol. 143, no. 4, pp. 747–794, 2011.

[16] D. d'Humiéres, I. Ginzburg, M. Krafczyk, P. Lallemand, and L.-S. Luo, "Multiple-relaxation-time lattice Boltzmann models in three dimensions," *Philosophical Transactions of the Royal Society A: Mathematical, Physical and Engineering Sciences*, vol. 360, no. 1792, pp. 437–451, 2002.

[17] P. Lallemand and L.-S. Luo, "Theory of the lattice Boltzmann method: dispersion, isotropy, Galilean invariance, and stability," *Physical Review E*, vol. 61, no. 6, pp. 6546–6562, 2000.

[18] S. G. Chen, C. H. Zhang, Y. T. Feng, Q. C. Sun, and F. Jin, "Three-dimensional simulations of Bingham plastic flows with the multiple-relaxation-time lattice Boltzmann model," *Science China Physics Mechanics and Astronomy*, vol. 57, no. 3, pp. 532–540, 2014.

[19] S. Chen and G. D. Doolen, "Lattice Boltzmann method for fluid flows," *Annual Review of Fluid Mechanics*, vol. 30, no. 1, pp. 329–364, 1998.

[20] S. Succi, H. Chen, and S. Orszag, "Relaxation approximations and kinetic models of fluid turbulence," *Physica A: Statistical Mechanics and its Applications*, vol. 362, no. 1, pp. 1–5, 2006.

[21] Z. Guo, C. Zheng, and B. Shi, "Discrete lattice effects on the forcing term in the lattice Boltzmann method," *Physical Review E*, vol. 65, no. 4, p. 046308, 2002.

[22] C. Körner, M. Thies, T. Hofmann, N. Thürey, and U. Rüde, "Lattice Boltzmann model for free surface flow for modeling foaming," *Journal of Statistical Physics*, vol. 121, no. 1-2, pp. 179–196, 2005.

[23] P. Prajapati and F. Ein-Mozaffari, "CFD investigation of the mixing of yield pseudo plastic fluids with anchor impellers," *Chemical Engineering & Technology*, vol. 32, no. 8, pp. 1211–1218, 2009.

[24] M. S. Huang, *The Application of Discrete Element Method on Filling Performance Simulation of Self-Compacting Concrete in RFC*, Ph.D. thesis, Tsinghua University, Beijing, China, 2010, in Chinese.